Energy Storage Materials 56 (2023) 192–204

Contents lists available at ScienceDirect

Energy Storage Materials

journal homepage: www.elsevier.com/locate/ensm

In-operando GC-MS: A new tool for the understanding of degradation processes occurring in electrochemical capacitors

Fabian Alexander Kreth, Lars Henning Hess, Andrea Balducci *

Friedrich-Schiller-University Jena, Institute for Technical Chemistry and Environmental Chemistry (ITUC) and Center for Energy and Environmental Chemistry Jena (CEEC Jena), Philosophenweg 7a, 07743 Jena, Germany

ARTICLE INFO

Keywords:
Aging
EDLCs
Electrolyte
GC-MS
Operando
Supercapacitor

ABSTRACT

In this work, we present an innovative design of an electrochemical three-electrode cell for *in-operando* gas chromatography-mass spectrometry analysis, which allows performing electrochemical measurements while probing and analyzing the liquid electrolyte in real-time. The presented cell shows similar electrochemical performance to commonly used lab-scale cells and can be utilized for the investigation of any kind of electrochemical system. The three-electrode configuration enables the differentiation of processes occurring at the respective positive or negative electrode. Investigating the aging of electrochemical cells, it is possible to obtain a detailed time-resolved insight into occurring decomposition processes. As a model case, we investigated aging processes occurring in an electric double-layer capacitor containing a one-molar solution of tetraethylammonium tetrafluoroborate in acetonitrile. Showing a time- and voltage-dependent evolution, decomposition products of the salt, solvent, and electrode were detected and assigned to aging processes occurring at the respective positive and/or negative electrode-electrolyte interphase. Used for the detection of soluble decomposition species within the electrolyte, *in-operando* gas chromatography-mass spectrometry is uniquely suited to be combined with techniques focused on the electrode and/or gas phase of electrochemical energy storage devices.

1. Introduction

Electrochemical energy storage devices, such as electrochemical capacitors and batteries, are widely used in today's society and enable the use of electric vehicles, electric mobile devices, and many more systems. However, such devices have limits regarding their respective specific energy, specific power, and lifetime. Increasing those parameters is therefore vital to meet society's growing demand for more efficient and more powerful energy storage systems [1,2].

When operated above their rated parameters aging processes occur within the electrolyte-electrode interphase of these devices. Primary aging processes of electrochemical capacitors include electrolyte-depleting and electrode pore-blocking side-reactions, mechanical detachment of the active material from the current collector (delamination), as well as internal cell pressure increase due to the evolution of volatile side-products. Typically, they are recognizable by capacitance fading and an increase of the equivalent series resistance (ESR) [3–5]. In batteries, occurring aging processes include parasitic side reactions, poor solid electrolyte interphase formation, dendrite formation, active material dissolution, electrolyte decomposition, delamination, as well as gas evolution, and thus pressure increase. Those processes result in capacity loss, power fading as well an increase of the ESR [6].

It is evident that being able to track and understand the occurring side reactions, which lead to cell aging, is of fundamental importance for the development of advanced energy storage devices. In the last years, various *in-situ/in-operando* techniques have been developed to investigate energy storage mechanisms, which may also be used to study respective aging processes [7–13]. In literature, the terms *in-situ* and *in-operando* are often freely exchanged with each other. Generally, they refer to techniques that enable the investigation of occurring processes at the place of their origin during operation (here: during an electrochemical measurement). However, a distinct differentiation between those two terms can be proposed: According to the Oxford English Dictionary, the term *in-situ* can be described as 'in its (original) place; in position/at the place or locality in question', whereas the term *in-operando* translates as 'working or operating' further distinguishes the additional temporal resolution of a measurement [14,15]. The successful application of *in-situ/in-operando* calorimetry [16–19], simultaneous thermal analysis (STA) [20], dilatometry [21,22], (pulsed) differential or online electrochemical mass spectroscopy (PEMS/DEMS/OEMS)

* Corresponding author.
E-mail address: andrea.balducci@uni-jena.de (A. Balducci).

https://doi.org/10.1016/j.ensm.2023.01.014
Received 18 July 2022; Received in revised form 9 January 2023; Accepted 10 January 2023
Available online 12 January 2023

[23–25], electrochemical quartz microbalance (EQCM) [26–33], (surface-enhanced) Raman spectroscopy (SERS, Raman) [34–38], attenuated total reflection Fourier transform infrared spectroscopy (ATR-FTIR) [37,39–44], nuclear magnetic resonance spectroscopy (NMR) [10,45–51], electrochemical atomic force microscopy (EC-AFM) [33,52–57], X-ray diffraction (XRD) [58–67], and X-ray photoelectron spectroscopy (XPS) [68–71], have been reported, just to mention a few. Among these techniques, *in-situ* STA is an effective technique to investigate the variation of heat flow, mass loss, internal resistance, and capacity/capacitance loss [20]. Measurements by PEMS/DEMS/OEMS enable the quantitative and qualitative analysis of evolving gases. The combination with *in-situ* dilatometry provides a powerful tool to investigate the nature and cause of the cell pressure built up [21–25]. EQCM enables precise tracking of mass changes during electrochemical measurements. By superimposing an applied constant potential with an electrochemical impedance spectroscopy (EIS) signal, it is possible to separate the broad EQCM response into individual anion, cation, and solvent molecule signals. Further, depending on configuration, geometrical and morphological changes as well as changes in the reaction mechanism (passive layer formation, decomposition) can be monitored [26–33]. Raman spectroscopy can provide information on the electrode structure, oxidation states, kinetics, chemical composition as well as lattice defects [34–38]. NMR provides the possibility to study ion configuration, ion confinement, ion dynamics, (de)solvation effects, and adsorption structure inside (nano)pores during electrochemical measurements [10,45–51]. XPS is a powerful tool for the investigation of the dynamics and stability of electrode-electrolyte interphases during polarization. Further, variation of oxidation states as well as electronic states (energy levels) can be monitored in real-time [68–71].

It is important to remark that, due to the nature of the different charge-storage mechanisms of electrochemical devices (faradic, capacitive, or pseudocapacitive), not every *in-situ/in-operando* technique can be applied for each case. Further, due to an open-cell design and/or required vacuum atmosphere within the analytical instrument, some techniques are limited to devices containing only ionic liquids, low-volatile organic, or aqueous electrolytes.

To the best of our knowledge, so far, only a few *in-situ/in-operando* techniques have been utilized for the investigation of aging processes occurring within non-aqueous electric double-layer capacitors (EDLCs, often referred to as supercapacitors). Due to safety concerns, especially the pressure increase occurring in EDLCs has been investigated using differential or online electrochemical mass spectroscopy (DEMS/OEMS). Hahn *et al.* investigated propylene carbonate (PC) based EDLCs. Here, carbon dioxide (CO_2), propene, and hydrogen (H_2) were detected as the major gaseous decomposition products. The formation of propene and H_2 was assigned to the reduction of the solvent at the negative electrode and the evolution of CO_2 was attributed to the solvent oxidation at the positive electrode [24]. Using *in-operando* dilatometry Hahn *et al.* recorded reversible and irreversible cell pressure changes at voltages up to 3 V for PC-based EDLCs. While cycling within a cell voltage window of 2.5 V, a reversible pressure decrease and increase during charge-discharge was determined, which the authors attributed to concentration-related volume changes of the electrolyte. When applying cell voltages above 2.5 V significant and irreversible gas evolution was observed [21]. Comparing different electrolytes Kötz *et al* showed that the extent of cell pressure build-up in EDLCs is strongly dependent on the stability of the respective solvents. Significant gas evolution was observed in γ-butyrolactone (GBL) at 2.5 V, in PC at 3.0 V, and in acetonitrile (ACN) at 3.25 V. The authors noted, that even though gas evolution in acetonitrile started at higher potentials than in propylene carbonate, PC showed significantly lower faradic currents than ACN (and GBL). Thus, attributing the higher leakage currents of ACN-based EDLCs to the formation of soluble electrolyte decomposition products instead of gas evolution reactions [22]. *In-operando* calorimetric measurements by Munteshari *et al.* revealed irreversible endothermic reactions for PC-based EDLCs when operated at cell voltages above 3 V, which has been assigned to the reductive decomposition of the solvent [16]. The measurements carried out by Hess *et al.* utilizing an *in-situ* STA cell correlate the variation of heat flow, mass loss, capacitance, and ESR during the aging of PC-based EDLCs [20]. It is important to point out, that these techniques focus on the analysis of evolving gases formed due to the reductive or oxidative degradation of the respective electrode-electrolyte interphase.

To achieve greater insight into the occurring aging processes within EDLCs, the use of *in-situ* or *in-operando* techniques that can supply information about the formation of non-gaseous decomposition products within these systems appears of great importance. However, to the best of our knowledge, these techniques have been not considered so far. Particularly, there is a lack of information about the decomposition processes taking place at the electrode-electrolyte interphase resulting in the formation of soluble, non-gaseous decomposition products.

Gas chromatography-mass spectrometry (GC-MS) allows the investigation of trace amounts of dissolved analytes within an appropriate solvent. Thus, it appears as an ideally suited technique for the investigation of formed decomposition products within the electrolyte of an electrochemical storage device. So far, several *post-mortem* investigations have been carried out utilizing this technique. An important example of this type of investigation is the work of Kurzweil and Chwistek, which addresses the degradation processes of the state-of-the-art electrolyte, a one-molar solution of tetraethylammonium tetrafluoroborate in acetonitrile (1 M $TEABF_4$ in ACN), in EDLCs. Considering their analytical findings, the authors postulated possible degradation mechanisms of acetonitrile and its oxidation products as well as the role of the respective salt. In the liquid phase of the aged electrolyte acetamide, acetic acid, several heterolytic compounds (e.g. pyrazines), and flouroacedic acid were successfully identified. The latter only at cell voltages as high as 6 V [3]. Recently, our group used *post-mortem* GC–MS measurements to investigate the degradation processes of electrolytes containing the salt 1,1-dimethylpyrrolidinium tetrafluoroborate ($Pyr_{11}BF_4$). When compared to the $TEABF_4$-based electrolyte, fewer decomposition products were observed at elevated cell voltages and temperatures [72].

However, to the best of our knowledge, the combination of electrochemical measurement with the *in-operando* analysis of the liquid electrolyte via GC-MS has not been reported so far, neither for electrochemical capacitors nor for batteries. Considering the amount of important information that could be acquired utilizing this type of *in-operando* cell, its development appears of great interest.

Herein, we present an innovative design of an electrochemical three-electrode cell for *in-operando* gas chromatography-mass spectrometry analysis of the liquid electrolyte of electrochemical energy storage devices. This cell supplies a detailed time-resolved insight into the formation and possible causes of degradation products. Further, the three-electrode configuration enables the differentiation between aging processes that occur at the positive and/or negative electrode. As a model case, the cell has been utilized to monitor the degradation processes occurring on activated carbon-based electrodes tested in combination with a non-aqueous electrolyte (1 M $TEABF_4$ in ACN) and on EDLCs containing the same electrodes and electrolyte.

2. Material and methods

The design of the developed electrochemical three-electrode *in-operando* GC-MS cell is shown in Fig. 1 [73]. The two current collectors of the cell consist of stainless steel (1.4301, X5CrNi18-10). Electrodes can be inserted into the cell and connected to the current collectors by applied pressure. Within the cell, they are separated by an in-house build spacer made from polyether ketone (PEEK) that has the shape of an O-ring with a cut on the top. The cell can be assembled in a two- or three-electrode configuration. In this latter case, a silver wire (Alfa Aesar, 99.9985%) can be used as a reference electrode. The cell body consists of polyetheretherketone (PEEK). All screw-type parts are sealed

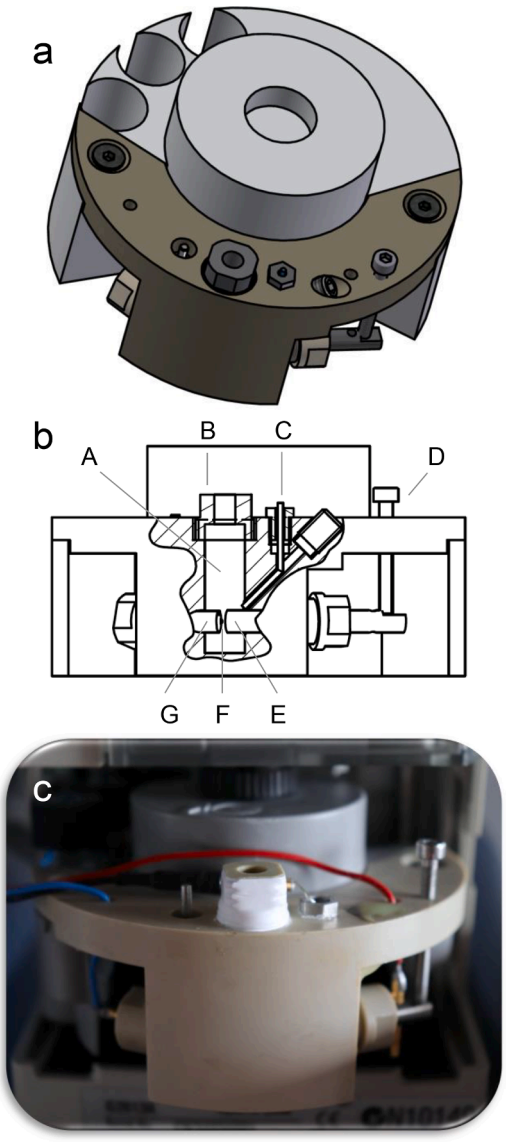

Fig. 1. Schematic drawings of the in-operando GC-MS cell (patent application 102022002412.8). [73] (a) 3D model, top view, (b) 2D model, side view. A) electrolyte chamber, B) top screw with piercable PTFE/silica septum, C) reference electrode (Ag-wire), D) adjustment screw, E and G) current collectors, and F) location of electrodes and spacer. (c) Picture of the assembled cell in a three-electrode configuration mounted inside the automated liquid sampler (ALS) and connected to a potentiostat/galvanostat.

either using gaskets and/or septa of fluoroelastomers (Viton®) or polytetrafluorethylene (PTFE). Glue, which has been used during the fabrication of the cell, is not in direct contact with the electrolyte. The cell can be assembled in an argon-filled dry box and filled with 1000-1200 µL electrolyte. The top of the cell is sealed using a PTFE/-white silica septum (Agilent) which allowed *in-operando* sampling of the electrolyte.

The cell can either be assembled symmetrically (two electrodes with almost identical mass), which is the case if a device is investigated, or asymmetrical (where one electrode is oversized in mass compared to the other), which is the case if processes occurring on one singular electrode are aimed to be investigated. The cell can be used with any type of electrochemical test. In the case of this study, the cell has been electrochemically cycled utilizing the sequence described in Fig. 1 of Supplementary Information (SI). In the case of an asymmetric set-up (Fig. 1a of SI), the potential of the positive and/or negative electrode is controlled against the Ag/Ag^+ reference electrode. Depending on the investigated electrode the applied potentials are either positive or negative. Firstly, electrochemical impedance spectroscopy (EIS) was performed within the range of 500 kHz to 10 mHz. After that, three cycles of galvanostatic charging and discharging (GCD) at 1 A g^{-1} up to a set potential of 1 V (-1 V) vs. Ag/Ag^+ followed by a 1 h floating period at the previously set potential are conducted. After five repetitions the set voltage is increased by 0.25 V (-0.25 V), at which point the sequence is repeated. This is repeated until a voltage of 2.25 V (-2.25 V) vs. Ag/Ag^+ is reached. The measurement ended with a final EIS measurement. In the case of a symmetric set-up (Fig. 1b of SI) the cell voltage, measured between the positive and the negative electrode, is controlled. Starting with impedance spectroscopy, three cycles of galvanostatic charging and discharging (GCD) at 1 A g^{-1} up to a cell voltage of 2.0 V are performed, followed by a 1 h floating period at the previously set voltage. After five repetitions the set voltage is increased by 0.5 V, at which point the sequence is repeated. This procedure is repeated until a voltage of 4.5 V is reached. The measurement ended with a final EIS measurement. During both procedures, each 5 h of floating (so after EIS measurement, 5 respective cycles of charge-discharge and floating at one potential) a sample of the liquid electrolyte is automatically taken via the automated liquid sampler, injected, and analyzed via GC-MS. After the injection of the sample mass spectra were continuously obtained. Different analytes will be separated via gas chromatography at which point they reach the mass spectrometer. When those analytes reach the MS, the obtained mass spectra can be compared with NIST databases and possible decomposition products can be identified.

To highlight the benefits of *in-operando* detection the same electrochemical aging protocol has been performed utilizing *post-mortem* X-cells, previously described in earlier publications [72,74,75]. Those cells display a similar design to the here presented in-operando GC-MS cell: A three-electrode set-up, where the working and counter electrode are separated by a 3 mm thick ring-shaped spacer. This spacer is made from PEEK and has a cutout on one side to enable better diffusion of the degradation products from the electrode-electrolyte interphase to the bulk electrolyte. The electrolyte reservoir was filled with 1.2 mL of electrolyte.

From the GCD profiles, the equivalent series resistance (*ESR*) [Ω cm^2] can be calculated by:

$$ESR = \frac{\Delta V_{\mathrm{ESR}}}{I \cdot 2} \cdot A_{\mathrm{el.}} \tag{1}$$

where I is the applied current [$A_{\mathrm{el.}}$] and ΔV_{ESR} [V] is the voltage drop (ohmic drop) between the highest potential during the charge phase and the potential of the discharge phase after a time delay of 100 ms (or between the lowest potential during the discharge phase and the potential of charge phase after a time delay of 100 ms) [76].

The specific capacitance *C* [F g^{-1}] is given by:

$$C_{\mathrm{ch./dis.}} = \frac{I}{m \cdot \left(\frac{\mathrm{d}V(t)}{\mathrm{d}t}\right)_{\mathrm{ch./dis.}}} \tag{2}$$

where *m* is the active mass of the electrodes [g] and $\mathrm{d}V(t)/\mathrm{d}t$ [V s^{-1}] is the slope of the charge/discharge curve [77].

Electrochemical testing was performed with an SP-150 from Biologic. The gas chromatographic and mass spectrometric measurements were performed with an Agilent 5977A EI-MSD - 7890 B GC System (mass range 1.6 - 1050 amu). The system is equipped with an Agilent 7683 Series automatic liquid sampler and an HP-5ms column from Agilent (30 m, ID 0.25, DF 1, Temp range -60 to 325/350°C). The applied temperature ramp was from 40°C to 280°C at 15 K min^{-1} and the respective carrier-gas flow (He) was set to 1 mL min^{-1} at a split ratio of 2:1. The respective injection volume of liquid samples has been set to 1 µL by a 10 µL syringe. The obtained mass spectra were compared to a NIST/EPA/NIH Mass Spectral Library (version 2.2, build June 10, 2014), with the determined analytes showing a match probability higher

than 60% displayed in the respective total ion chromatograms (TICs). The TICs were subjected to background subtraction and baseline correction.

Composite carbon electrodes were produced by mixing activated carbon (Kuraray YP-50F, 90 wt.%), carbon black (IMERYS Super C65, 5 wt.%), and binder (Dow Chemical Walocell sodium carboxymethylcellulose, NaCMC, 5 wt.%) in 8 ml water. This slurry was stirred in a dissolver for 30 min until it yielded a homogenous suspension. This suspension was cast on aluminum foil with a doctor blade set to 150 μm. From this foil 5 mm circular cutouts were made using an in-house made punch press. The average mass of active material per standard carbon electrode was 0.43 mg. Oversized carbon electrodes have been produced by mixing Kuraray YP-50F (85 wt.%) with IMERYS Super C65 (5 wt.%) and PTFE (10 wt.%) in 50 mL ethanol (EtOH). After stirring for 2 h and heating to 80°C the suspension has been transferred onto a glass plate and rolled flat until a thickness of 1-2 mm is reached. 5 mm free-standing electrodes were punched and dried. The average mass of these electrodes was 6 ± 0.5 mg.

As the electrolyte, a one molar solution of tetraethylammonium-tetrafluoroborate ($TEABF_4$) (Sigma Aldrich) in acetonitrile (ACN) (Sigma Aldrich) was chosen. The electrolyte was prepared in an Argon-filled dry box (Labmaster Pro, MBraun). Drying the solvent using molar sieves 3 Å (Köstrolith) resulted in an electrolyte with a water concentration below 20 ppm, measured by Karl Fischer Titration. All used solid materials as well as the chosen salt were dried in a vacuum glass oven at elevated temperatures.

3. Results and discussion

The cell considered in this work can be easily implemented into existing automated liquid samplers of a gas chromatograph coupled mass spectrometer. By automated sampling of the liquid electrolyte during electrochemical measurement, the cell enables the time-resolved detection of decomposition products and thus allows the investigation of specific aging processes within electrochemical devices, e.g. supercapacitors and batteries. The implementation of a three-electrode configuration further permits the distinction of decomposition processes that occur on the respective negative and/or positive electrode.

It is important to remark that when developing such a cell certain requirements must be met:

1.) Impermeability – The cell has to be impermeable to liquids and gases.
2.) Piercability – The probe has to have access to the inner part of the cell (the electrolyte chamber) while maintaining impermeability for liquids and gases.
3.) Diffusion – Even though GC-MS can detect trace amounts of analytes, the diffusion of decomposition products from the electrode-electrolyte interphase to and within the electrolyte itself has to be achieved.
4.) Mounting – The cell has to be freely exchangeable with the original turret of the automated liquid sampler and/or be installed in other autosampler systems in such a way that direct probing is possible.
5.) Durability – The cell needs to endure elevated currents and potentials as well as an aggressive chemical environment.
6.) Performance – The cell has to show a similar electrochemical performance as commonly used lab-scale cells (e.g. Swagelok®-type cells or coin-cells).

The fulfillment of all these requirements is important to guarantee reproducible electrochemical behavior. Further, it generates an environment in which the degradation processes generated during the electrochemical tests are not affected by external agents, e.g. air or moisture. The cell presented in this study is fulfilling all these requirements and, therefore, is suitable for the investigation of the degradation process occurring at the electrode-electrolyte interphase of activated carbon-based EDLCs.

Initially, we investigated the impact of the potential on the aging of activated carbon-based electrodes tested in 1 M $TEABF_4$ in ACN. The protocol utilized for these tests is described in detail in the experimental section. Fig. 2 shows the electrochemical behavior observed for an activated carbon electrode subject to increasing potential (from 1 to 2.25 V Ag/Ag^+). Fig. 2a shows the specific capacitance (F g^{-1}) and equivalent circuit resistance (ESR, Ω cm^2) of the electrode as a function of the accumulated floating time. As described above, after 5 h of floating the applied potential was increased by 0.25 V. From the figure it is evident that the capacitance, as well as the ESR, show stable values until a potential of 1.75 V vs. Ag/Ag^+ is reached. Interestingly with increasing applied positive potential the capacitance increases as well. This can be attributed to the increased participation of ions in the formation of the electric double layer due to a stronger electric field [78]. At potentials higher than 2 V vs. Ag/Ag^+ a sharp decrease of the capacitance and increase of the ESR is observed, indicating strong aging of the cell and thus the generation of decomposition products. Fig. 2b shows Nyquist diagrams of the obtained electrochemical impedance spectra. At the start of the measurements, an EDLC-like impedance spectrum is obtained (consisting of a small half circle followed by a steep increase of the imaginary part). It is evident, that with increasing floating time and potential this shifts slightly towards higher resistances. At 20 h of floating (set potential of 1.75 vs. Ag/Ag^+) the resistance sharply increases but still shows the characteristics of a lab-scale EDLC. As seen before, this changes at 20 h and a set potential of 2.00 V vs. Ag/Ag^+. Here the absence of a half-circle indicates a strong degradation of the electrode-electrolyte interphase and a strong increase of the internal resistances. Fig. 2c-e show a selection of galvanostatic charge-discharge (GCD) profiles of the positive electrode (red) and the negative oversized electrode (black) at 0 h, 15 h, and 30 h. At 0 h (set potential of 1 vs. Ag/Ag^+) and 15 h (set potential of 1.50 vs. Ag/Ag^+) the two electrodes show an ideal EDLC-like linear behavior. At 30 h (set potential of 2.25 vs. Ag/Ag^+) the profiles show a curved line. This again indicates strong degradation of the electrode-electrolyte interphase. It is evident, that the negative electrode shifts further towards negative potential when aging processes occur on the positive electrode. This is expected and can be attributed to the irreversible oxidation on the positive electrode, which results in an accumulation of electrons on the negative electrode. This shift can be neglected as long as the negative electrode is within the stability window of the investigated system.

Fig. 3 shows the three-dimensional time-resolved total ion chromatograms (TICs) of the *in-operando* GC-MS measurements which were obtained during aging tests of the positive electrode. TICs display the accumulated intensity (rel. abundance) across the detected range of masses at every point during analysis as a function of the time (retention time of the analytes, t_R). Thus, each peak correlates to a specific mass spectra and indicates one specific degradation product. The characteristic retention time of each compound does not change as long as the parameters of the analysis do not change. By comparing the obtained TICs it is evident that the first peaks arise at 1.75 vs. Ag/Ag^+ and that the height and area increase with increasing potential. Further, the total amount of detected signals increases with increasing potential. This clearly shows the stronger degradation at higher potentials. During this aging test, four degradation products were identified and could be assigned to aging processes occurring at the positive electrode: acetamide (t_R 8 min), N-ethyl-acetamide (t_R 12 min), 2,4,6-trimethyl-1,3,5-triazine (t_R 12.5 min) and diacetamide (t_R 14 min). The corresponding mass spectra are shown in Fig. 2a-e of SI. Acetamide, N-ethyl-acetamide, and diacetamide are formally hydrolysis products of the chosen solvent acetonitrile [3]. Since the electrolyte shows a water content below 20 ppm and the cell has been assembled in an inert atmosphere, it is plausible to attribute the origin of oxygenated decomposition products to reactions of acetonitrile with the =O/-OH/-COOH and -COOR surface functions of the used activated carbon material [79–81]. Further, it is

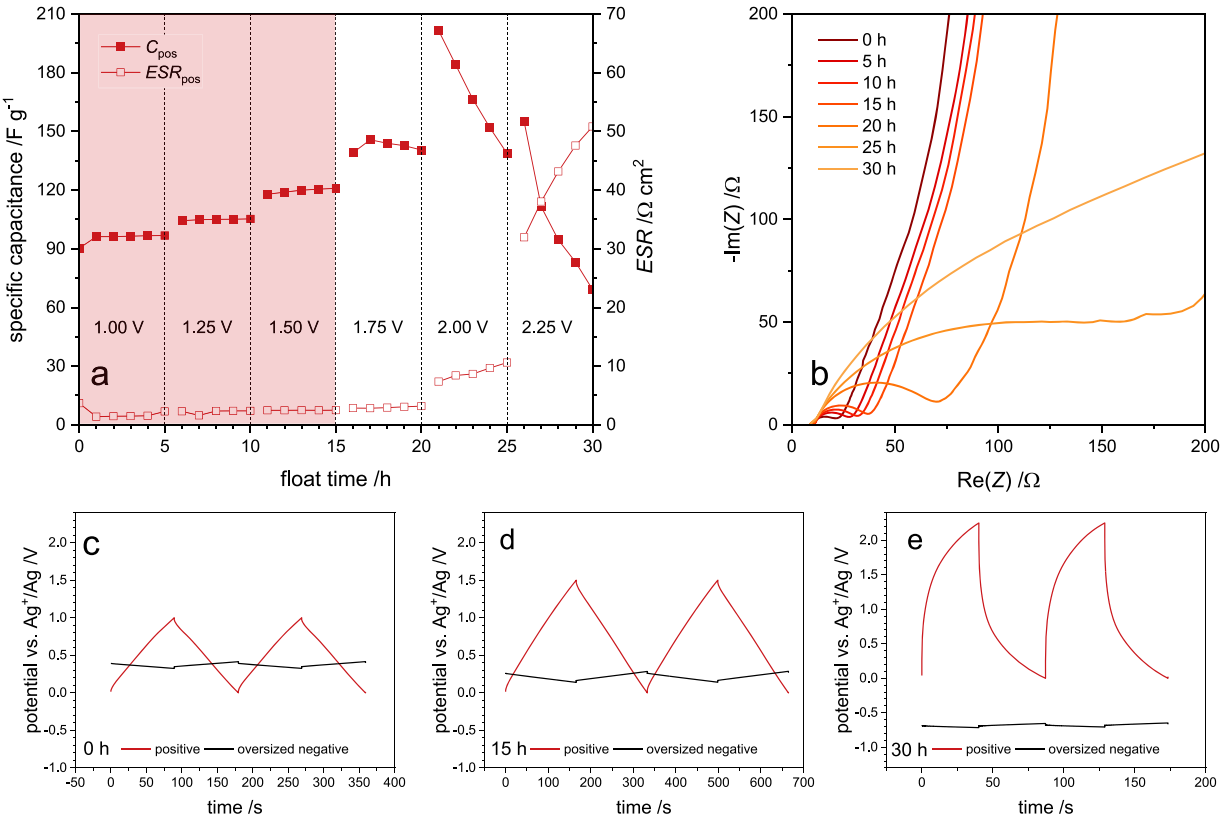

Fig. 2. Electrochemical performance of an aging test of a positive activated carbon electrode: (a) variation of the specific capacitance (F g^{-1}) and equivalent circuit resistance (ESR, Ω cm^2) as a function of the accumulated floating time; (b) Nyquist diagrams of the obtained electrochemical impedance spectra; (c-e) selection of galvanostatic charge-discharge profiles of the positive electrode (red) and the negative oversized electrode (black) at 0 h, 15 h, and 30 h.

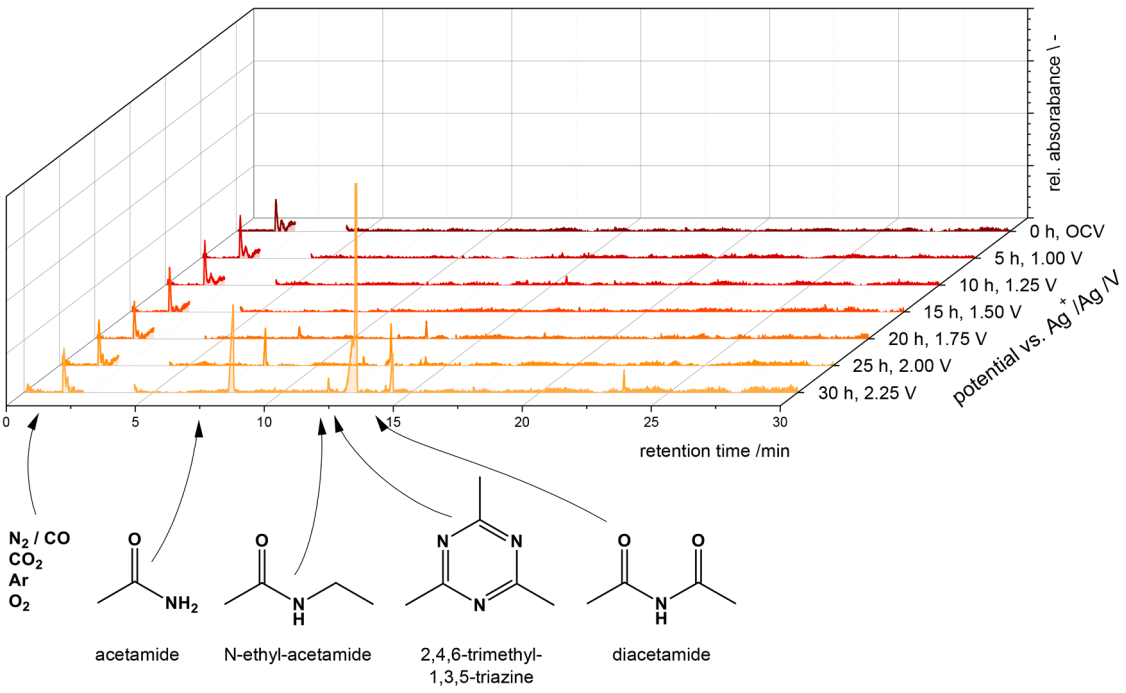

Fig. 3. TICs of the *in-operando* GC-MS measurements obtained during aging tests of the positive electrode. Four degradation products were identified: acetamide (t_R 8 min), N-ethyl-acetamide (t_R 12 min), 2,4,6-Trimethyl-1,3,5-triazine (t_R 12.5 min), and diacetamide (t_R 14 min).

possible to attribute their origin to reactions of acetonitrile with the hydroxy and ester groups of the utilized carboxymethylcellulose (CMC)-binder of the respective working electrode [82,83]. However, at this point, evidence regarding the influence of surface chemistry and the electrode composition can not be provided. 2,4,6-Trimethyl-1,3,5-triazine is a cyclotrimerization product of acetonitrile which has

been reported to form under very harsh conditions (high temperature, high pressure, strong acidic or alkaline media) [84–86]. The application of catalysts, such as lanthanum and yttrium triflate, trifluoromethanesulphonic acid, and mesoporous graphitic carbon nitride, show a successful decrease of the normally very high activation energies [87–89]. It is, therefore, reasonable to suppose that the use of high electrochemical potentials in combination with a porous carbon surface can generate an electrocatalytic environment, which can promote the reaction of acetonitrile toward triazines. Interestingly no fluor-containing decomposition products were detected during the aging of the positive electrode indicating electrochemical stability of the BF^- anion within the applied potential range. However, this is consistent with other publications which show that electrochemical fluorination (Simons' process) requires cell voltages higher than 5 V [3,90,91]. Further, potentially formed fluorodecomposition products may remain at the electrode surface, precipitate from solution, or in the case of gases (HF, *m/z* 20) outgas and/or do not dissolve within the respective limit of detection (LOD) of the device.

Afterward, the impact of the stability of the activated carbon electrodes subjected to decreasing potential (from -1 to -2.25 V Ag/Ag^+) was considered (Fig. 4). Fig. 4a shows the specific capacitance (F g^{-1}) and equivalent circuit resistance (ESR, Ω cm^2) as a function of the accumulated floating time. As shown, capacitance fading starts occurring at -1.75 V vs. Ag/Ag^+, whereas an increase of the ESR is already seen at -1.50 V vs. Ag/Ag^+. Thus, it can be assumed, that aging processes start occurring at -1.50 V vs. Ag/Ag^+, but the duration of the floating step is too short for a significant decrease of electrode surface area which would result in a loss of capacitance. At potentials lower than -2.00 V vs. Ag/Ag^+, the cell shows such severe decomposition that neither capacitance nor ESR could be determined. Similar to the aging test of the positive electrode, but not as strong, the capacitance increases with increasing applied negative potential until aging processes dominate. Fig. 4b is comparing electrochemical impedance spectra of the negative electrode in a Nyquist diagram during the aging test. The characteristic EDLC-like progression of the graph degrades over time shifting towards higher resistances. Confirming the presence of increased aging processes at potentials lower than -1.50 V vs. Ag/Ag^+, the deterioration of the initial course of the impedance spectra indicates a strong degradation of the electrode-electrolyte interphase and a strong increase of the internal resistances. Fig. 4c-e show galvanostatic charge-discharge (GCD) profiles of the negative standard electrode (blue) and the positive oversized electrode (black) at 0 h (set potential of -1.00 V vs. Ag/Ag^+), 15 h (set potential of -1.50 V vs. Ag/Ag^+), and 25 h (set potential of -2.00 V vs. Ag/Ag^+). Unfortunately, due to the complete deterioration of the cell, showing GCD profiles at 30 h (set potential of -2.25 V vs. Ag/Ag^+) is not possible. Here capacitance fading can be observed by the change of the linear slope (which is characteristic for EDLCs) towards a more curved slope. As it has been observed before, with increasing aging of the negative electrode, the positive oversized electrode experiences a drift toward more positive potentials. This is can be attributed to the irreversible reduction processes at the negative electrode and the resulting accumulation of positive charges (electron deficiencies) at the positive electrode. As long as the oversized positive electrode is within the positive stability limit, this can be neglected.

Fig. 5 is comparing the obtained time-resolved TICs taken in-operando during the aging test of the negative electrode. The first significant peaks arise at 25 h (set potential of -1.75 vs. Ag/Ag^+) which increase both in height and area as well as in number with increasing floating time and negative potential. During the aging test, six degradation products were identified and could be assigned to aging processes occurring at the negative electrode: ethylene (t_R 2 min), triethylamine (t_R 6 min) acetamide (t_R 8 min), N-ethyl-acetamide (t_R 12 min), 2,4,6-trimethyl-1,3,5-triazine (t_R 12.5 min) and 3-aminocrotononitrile (t_R 17 min). The corresponding mass spectra are shown in Fig. 3a-f of SI.

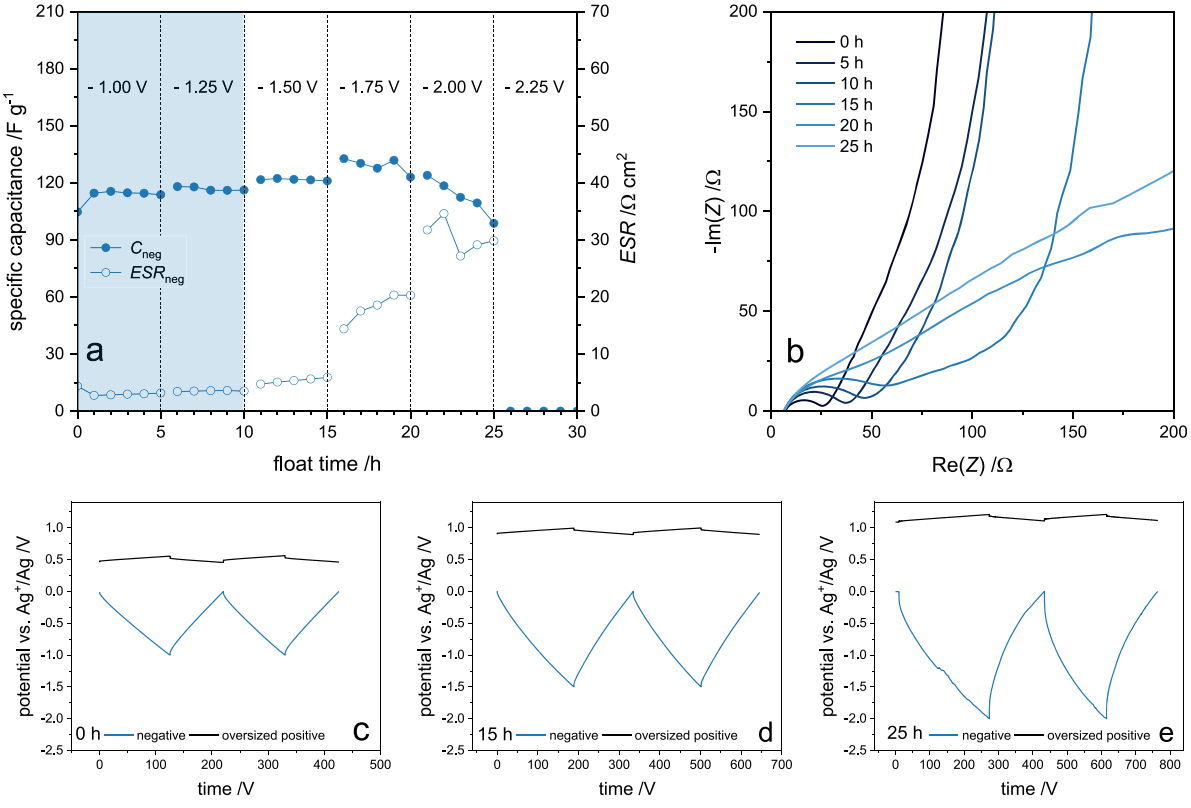

Fig. 4. Electrochemical performance of an aging test of a negative activated carbon electrode: (a) variation of the specific capacitance (F g^{-1}) and equivalent circuit resistance (ESR, Ω cm^2) as a function of the accumulated floating time; (b) Nyquist diagrams of the obtained electrochemical impedance spectra; (c-e) selection of galvanostatic charge-discharge profiles of the negative electrode (blue) and the positive oversized electrode (black) at 0 h, 15 h, and 25 h.

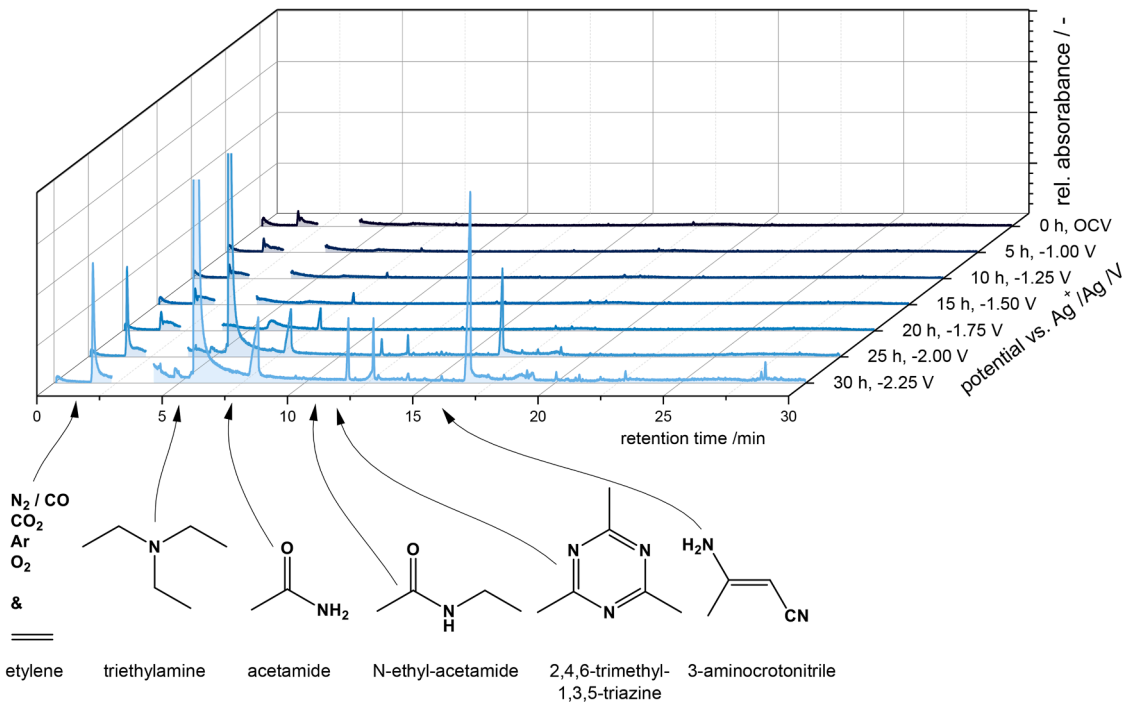

Fig. 5. TICs of the *in-operando* GC-MS measurements obtained during aging tests of the negative electrode. Six degradation products were identified: ethylene (t_R 2 min), triethylamine (t_R 6 min) acetamide (t_R 8 min), N-ethyl-acetamide (t_R 12 min), 2,4,6-trimethyl-1,3,5-triazine (t_R 12.5 min) and 3-aminocrotononitrile (t_R 17 min).

Interestingly, when compared with the aging test of the positive electrode, three decomposition products are formed at both, the positive and the negative electrode, and three additional decomposition products are formed exclusively at the negative electrode. Acetamide and N-ethyl-acetamide are detected for both aging tests, forming at potentials higher than 1.75 V vs. Ag/Ag^+ and lower than -1.50 V vs. Ag/Ag^+. Thus, the potential drift of the respective oversized counter electrode down to -0.8 and up to 1.2 V vs. Ag/Ag^+ can be neglected as a possible cause for the formation of those decomposition products. We propose, that both, an excess of negative and positive charges at the electrode surface, resulting in sufficiently high positive and negative potentials, can initiate the reaction of acetonitrile with oxygen-containing activated carbon and/or CMC-binder surface functions to acetamide derivates. 2,4,6-trimethyl-1,3,5-triazine is detected for both aging tests which can be caused by similar reasons. Interestingly, 3-aminocrotononitrile, which can be attributed to the dimerization of acetonitrile, is only found during aging of the negative electrode. Since one can assume the dimer to be an intermediate product of the cyclotrimerization of acetonitrile, this indicates that the cyclotrimerization occurring during the aging of the respective positive or negative electrode proceeds via two different reaction pathways. Two of the decomposition products formed exclusively during aging of the negative electrode are ethylene and triethylamine, which can be attributed to the degradation of the tetraethylammonium cation (TEA^+). This reaction is known as a Hofmann elimination, where quaternary amines form tertiary amines and alkenes while a proton gets eliminated [3,92].

Fig. 6 displays the electrochemical data obtained during aging test of a symmetrical cell (containing two activated carbon electrodes with almost identical mass) according to the protocol displayed in Fig. 1b of SI. Here, the cell voltage (voltage difference between the potential of the positive and negative electrode) is controlled whereas the respective electrode potential is free to drift. This simulates the aging behavior of commercial devices since they are mostly built in a two-electrode configuration. Here, to achieve a better comparison, Fig. 6a shows the capacitance retention of the cell, the positive and the negative electrode as well as the respective equivalent circuit resistance (ESR, Ω cm^2) as a function of the accumulated floating time. Interestingly, strong capacitance fading occurs already at 3.00 V cell voltage. This can be explained by the respective potentials of the positive and negative electrode during this measurement. Fig. 6c-e show galvanostatic charge-discharge (GCD) profiles of the cell (grey), the positive (red), and the negative electrode (blue) at 0 h (set voltage of 2.00 V), 15 h (set voltage of 3.00 V), and 30 h (set voltage of 4.50V). At 3.00 V cell voltage, the positive electrode experiences a potential of approximately 2 V vs. Ag/Ag^+, whereas the negative electrode only experiences a potential of approximately -1 V vs. Ag/Ag^+. This is even more extreme during prolonged aging. After 30 h of floating (at a cell voltage of 4.50 V), the positive electrode reaches potentials as high as 3 V vs. Ag/Ag^+, whereas the negative electrode stays above -1.5 V vs. Ag/Ag^+. Thus, it can be concluded, that aging of a symmetric EDLC with an electrolyte consisting of 1 M $TEABF_4$ in ACN is mainly caused by decomposition processes occurring at or within the positive electrode-electrolyte interphase. This behavior can also be seen in the ESR increase of the positive electrode when compared with that of the negative (Fig. 6a) and is consistent with the aging behavior of acetonitrile-based EDLCs reported in literature [5]. Electrochemical impedance spectra of the cell are shown in Fig. 6b as Nyquist diagrams. The increase in internal resistance during increasing floating time corresponds well with the capacitance decrease and ESR increase obtained from the galvanostatic cycling. The characteristic EDLC-like course of the graph degrades at voltages higher than 3.00 V (15 h of floating) indicating strong aging of the device.

The total ion chromatograms of the aging test of a symmetrical cell are compared in Fig. 7. First peaks, indicating the presence of decomposition products, arise already at 3 V cell voltage. The total amount, height, and area of the respective peaks increase with increasing potential, indicating stronger degradation at higher cell voltages. Four degradation products were identified: acetamide (t_R 8 min), N-ethyl-acetamide (t_R 12 min), 2,4,6-Trimethyl-1,3,5-triazine (t_R 12.5 min), and diacetamide (t_R 14 min). The corresponding mass spectra are shown in Fig. 4a-e of SI. The observed decomposition products coincide with those of the aging test of the positive electrode, indicating that aging of this device is primarily caused by the decomposition of the positive

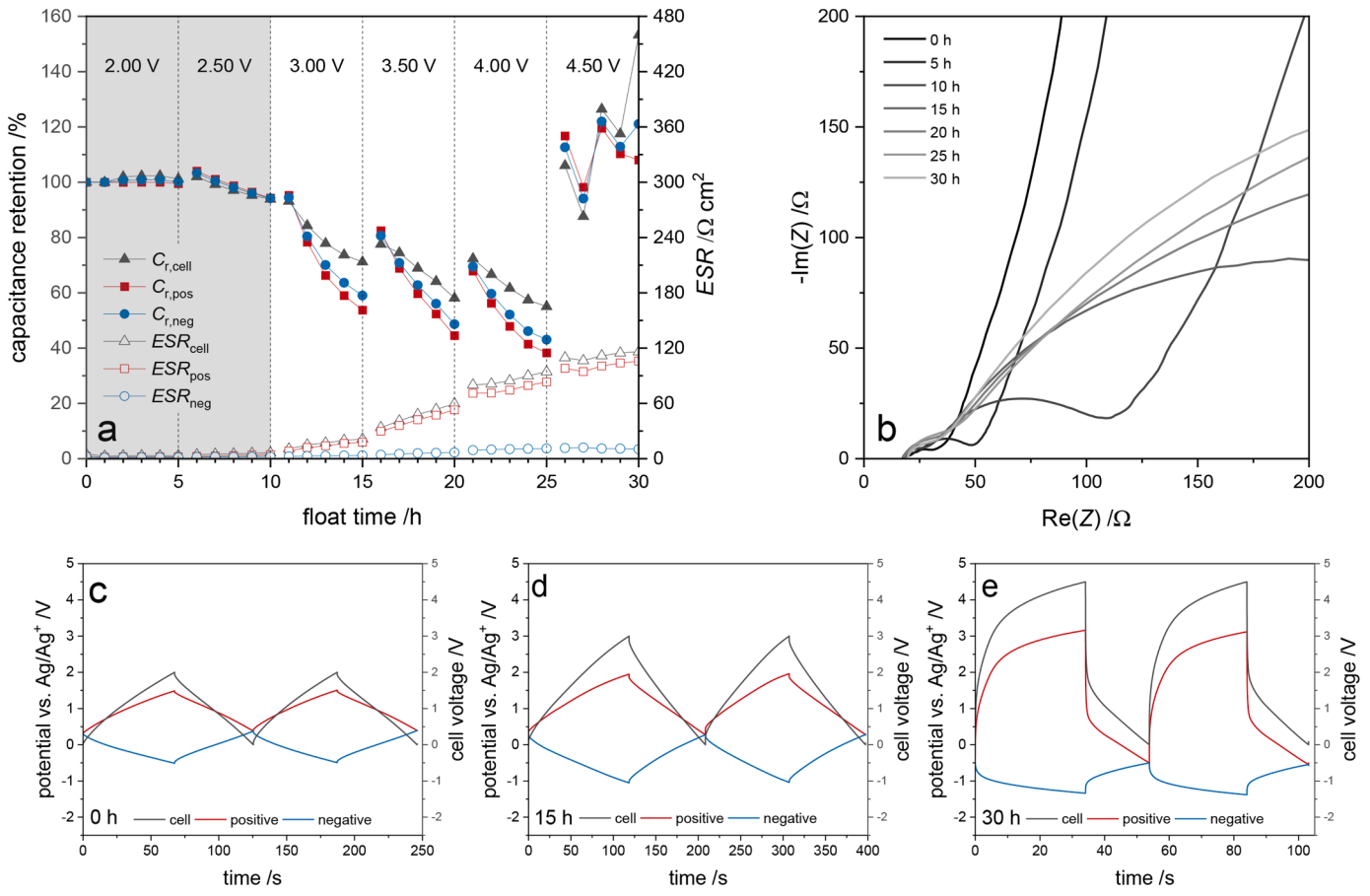

Fig. 6. Electrochemical performance of an aging test of a cell consisting of two activated carbon electrodes (positive and negative) and one Ag-reference electrode. Cell voltage (grey) is controlled between the respective positive (red) and negative (blue) electrode potential. Electrode potentials are measured against an Ag/Ag^+ reference electrode. (a) Variation of specific capacitance (F g^{-1}) and equivalent circuit resistance (ESR, Ω cm^2) as a function of the accumulated floating time; (b) Nyquist diagrams of the obtained electrochemical impedance spectra of the cell; (c-e) selection of galvanostatic charge-discharge profiles of the positive electrode (red), the negative electrode (blue), and the cell voltage (grey) at 0 h, 15 h, and 30 h.

electrode-electrolyte interphase.

It is important to observe that utilizing the cell proposed in this work is also possible an *in-operando* detection of the various decomposition products forming within EDLCs. Fig. 8 shows the changes over time of the TIC signals that have been observed in the aging test. The increase in peak area is directly correlated to the increase in the concentration of the corresponding decomposition product. The latter can be indirectly determined by performing a calibration of each analyte. This highlights that the use of *in-operando* GC-MS detection can enable real-time qualitative and quantitative analysis of degradation products occurring within a respective electrochemical device while electrochemical measurements are performed.

With the aim to compare the *in-operando* investigation with a "classical" offline detection, the electrochemical aging protocol considered above has been performed using *post-mortem* X-cells, previously described in an earlier publication [72]. Here, the electrolyte is sampled only once, at the end of the measurement. These X-cells display a similar design to that of the here presented *in-operando* GC-MS cell. Even though their electrochemical performance is inferior to that of the developed *in-operando* cell, it is possible to validate the reported results (see Figs. 5-7 of SI). However, the main drawbacks of using traditional *post-mortem* analysis are clear: If one would like to gain the same amount of results obtained with the *in-operando* cell one (a) would have to assemble far more cells and (b) cannot continue electrochemical measurements after analyzing the electrolyte sample.

The results obtained with the *in-operando* GC-MS cell are interesting and important for several reasons. First, they confirm that in ACN-based EDLCs the positive electrode is the main driving force for the aging of these devices [5]. Furthermore, they show that the reactions involving the ACN solvent are the main sources of degradation in these EDLCs. Decomposition reactions involving the conducting salt occur on the negative electrode at a rather low potential and have a minor impact on the overall aging process. Scheme 1 is illustrating an overview of the possible decomposition reactions taking place in the investigated systems based on the findings reported above. For the first time, it was possible to observe that the degradation reactions involving acetonitrile are mainly caused by interactions between this solvent and the oxygen-containing surface functions of the activated carbon and/or the used binder. These interactions can occur at both electrodes when an excess of charges (positive or negative) is generated at the electrode-electrolyte surface. Regardless of the polarity of the electrode, the reactions generated by these interactions are leading to the formation of acetamide and its derivate N-ethyl-acetamide. Further, the cyclotrimerisation of acetonitrile forming 2,4,6-trimethyl-1,3,5-triazine is observed at both electrodes as well. Considering these results, it is evident that the presence of surface functionalities has a dramatic impact on the stability of EDLCs. Another important result of these investigations is the possibility to identify the potentials at which the positive and negative electrodes of ACN-based EDLCs begin to age. We showed that the first degradation processes on the positive electrode are occurring at 1.75 V vs. Ag/Ag^+, while those of the negative at −1.50 V vs. Ag/Ag^+. Generally, in ACN-based symmetric EDLCs, the positive electrode is the first one that reaches this limit and, for this reason, is the one that most influences the overall degradation process in these

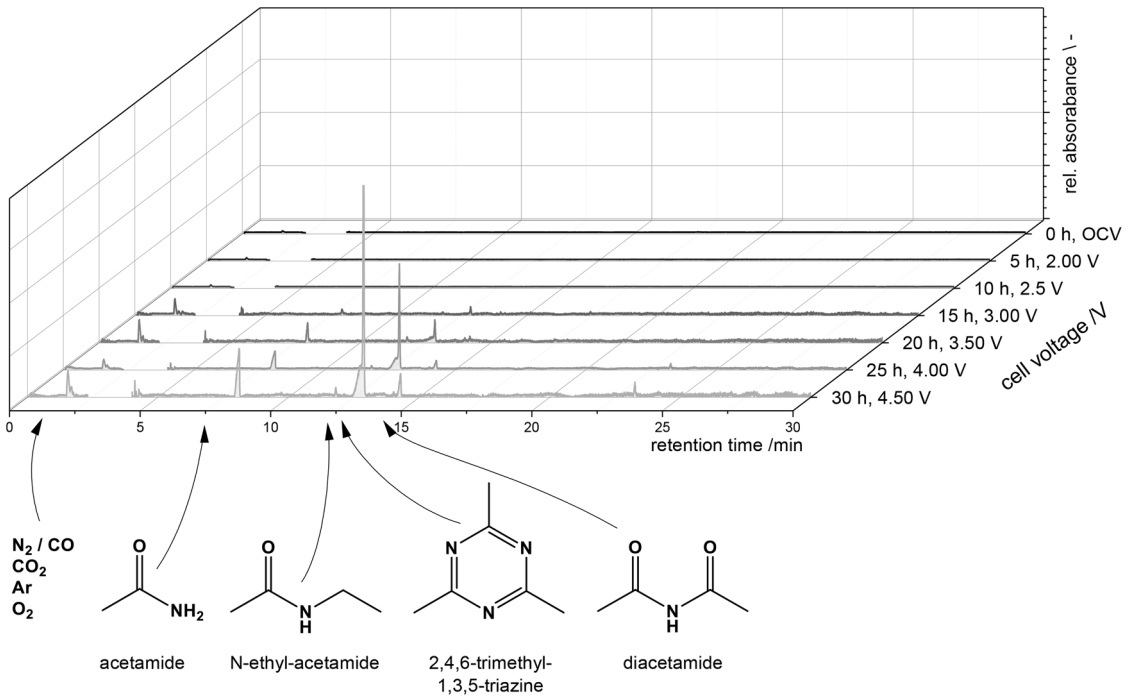

Fig. 7. TICs of the in-operando GC-MS measurements obtained during aging tests of a symmetric EDLC. Four degradation products were identified: acetamide (t_R 8 min), N-ethyl-acetamide (t_R 12 min), 2,4,6-Trimethyl-1,3,5-triazine (t_R 12.5 min), and diacetamide (t_R 14 min). The observed decomposition products are the same as in the aging test of the positive electrode, indicating that aging of this device is primarily caused by the decomposition of the positive electrode-electrolyte interphase.

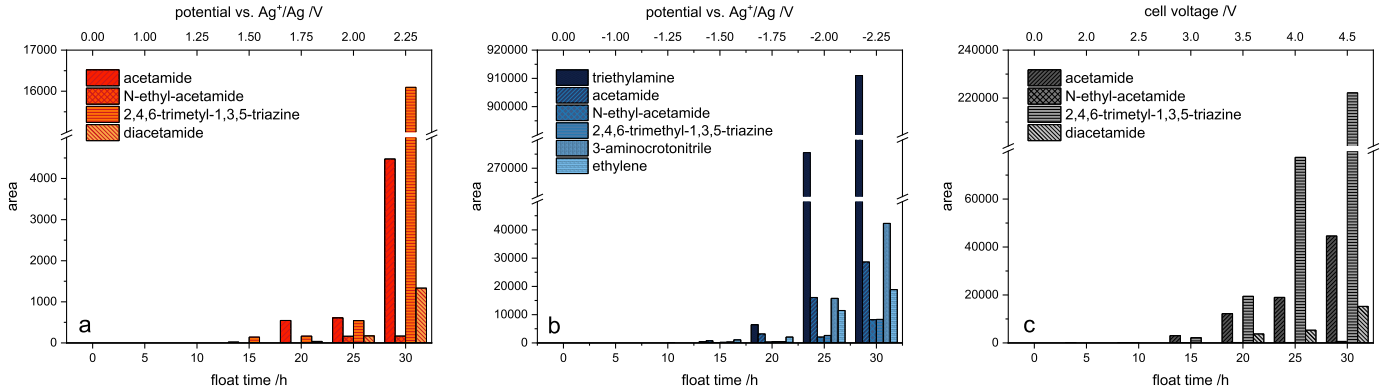

Fig. 8. Integrated areas of the corresponding TIC signals obtained during aging test of (a) the positive electrode, (b) the negative electrode, and (c) of the symmetric EDLC. An increase in peak area indicates a higher concentration of respective decomposition products. However, at this point, no information regarding their absolute concentration can be given (requires calibration of peak area with each analyte).

devices. Finally, the results of these investigations highlight a novel aspect related to the electrode-electrode interface in EDLC, namely, the possibility of generating electrocatalytic environments, which can promote the formation of compounds, such as triazines, that require very high activation energy to be formed.

Further, it is important to highlight, that the obtained results are comparing very well with those reported in previous works, which have been made utilizing electrochemical and *post-mortem* analytical techniques for the investigation of aging processes occurring within EDLCs. Ruch *et al.* conducted 500 h long floating experiments at 3.5 V cell voltage with symmetrical EDLCs containing the same electrolyte used in this study. Their results indicate a much higher capacitance loss and increase of the ESR for the positive electrode than for the negative electrode [5]. As can be seen in Fig. 6 a similar aging behavior has been reported in this work. Among other techniques, Kurzweil and Chwistek used post-mortem GC-MS for the analysis of aged electrolytes consisting of 1 M $TEABF_4$ in ACN. Within the liquid phase, they were able to identify acetamide, acetic acid, several heterolytic compounds (e.g. pyrazines), and flouroacedic acid. The latter only at cell voltages as high as 6 V [3]. Similar decomposition products were reported within this manuscript. However, with the implementation of *in-operando* probing of the electrolyte, we were further able to distinguish between aging processes occurring at the positive or negative electrode and determine the potentials at which the respective electrodes begin to age. Further, in contrast to the experimental set-up of Kurzweil and Chwistek, the here presented *in-operando* GC-MS cell strongly resembles other common electrochemical lab-scale cells (e.g. Swagelok®-type cells) in performance as well as design.

With an emphasis on the supercapacitor electrodes, carbon materials, and surface functionalities Azaïs *et al.* [79], Zhu *et al.* [93], Bittner *et al.* [94], and Liu *et al* [81,95]. Published several studies concerning possible aging mechanisms of ACN-based EDLCs. Azaïs *et al.* showed that occurring capacitance losses and resistance increases are related to the decomposition of the electrolyte onto the surface of the active carbon

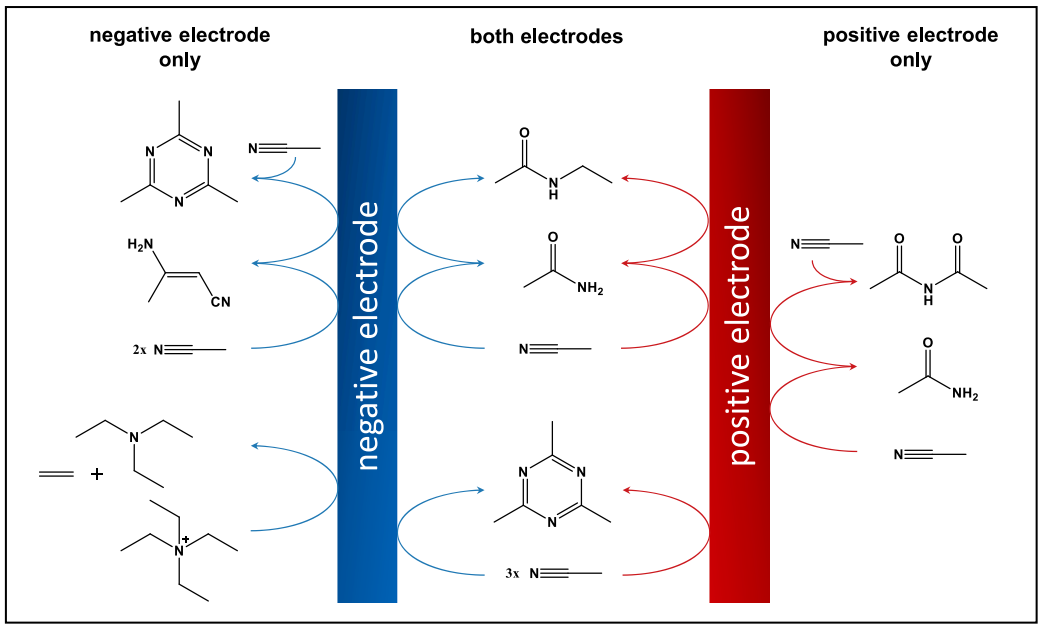

Scheme 1. Possible decomposition reactions occurring within an EDLC containing 1 M TEABF4 in ACN as electrolyte at the positive and/or negative electrode-electrolyte interphase. Acetamide, N-ethyl-acetamide, and 2,4,6-trimethyl-1,3,5-triazine are formed during the aging of both electrodes. Diacetamide is only formed during the aging of the positive electrode, whereas ethylene, triethylamine, and 3-aminocrotononitrile are only formed during the aging of the negative electrode. The presence of 3-aminocrotononitrile during aging at the negative electrode indicates, that the cyclotrimerization of acetonitrile occurring during the aging of both electrodes proceeds via two different reaction mechanisms. One, at the negative electrode, which forms the intermediate acetonitrile dimer (3-aminocrotononitrile), and one, at the positive electrode, which directly forms the triazine derivate.

material, creating surface defects and decreasing porosity. Here, acidic surface functionalities and water traces inside the electrolyte cause and increase the aging of the device. [79] Zhu *et al.* and Bittner *et al.* identified polymerization products from acetonitrile (pyridine, amines, and polyacetonitrile) as well as traces of nitrogen, fluorine, and oxygen on both electrodes. Here, the positively polarized electrode suffered more from degradation processes than the negative as well. While the carbon material of the negative electrode gets partially reduced and forms CH groups, the carbon material of the positive electrode gets oxidized while incorporating nitrogen, fluorine, and oxygen and thus forming various surface functionalities (especially carboxyl species). Further, the formation of reactive BF_4^- radicals which cause fluorination and HF formation is proposed. [93,94] Liu *et al.* investigated the influence of the type of carbon material on the aging mechanisms. Especially the surface functional group content of the positive electrode was reported to be decisive. The authors proposed hydrolysis of BF_4^- to HF-BF_3 and HF at the positive electrode in the presence of water traces which caused the formation of defects within the carbon network. The observed defects at the negative electrode have been explained by the partial diffusion of HF-BF_3 from the positive to the negative electrode. Those defects can further react resulting in the formation of surface functionalities such as carboxylic, anhydride, lactone, ether, phenol, and carbonyl groups. Further, soluble polyacetonitrile oligomers are created which caused the yellow coloration of the electrolyte [81,95]. Considering the aforementioned publications it is evident that the results obtained by *in-operando* GC-MS measurements of the liquid electrolyte are in good agreement with the investigations focused on the supercapacitor electrode materials. Both approaches show that the degradation of the positive electrode-electrolyte interphase is the primary cause of aging. Further, polymerization products of acetonitrile were detected in both, the electrode and the electrolyte. Additionally, *post-mortem* investigations of aged electrodes reveal surface defects, decreases porosity, and traces of fluorinated compounds, which were caused by the degradation of the BF_4^- to HF-BF_3 and HF at the positive electrode. This process has not been observed by analyzing the electrolyte itself. This strengthens the hypothesis that formed fluorodecomposition products remain at the electrode surface, precipitate from solution, or in the case of gases (HF, m/z 20) outgas and/or do not dissolve within necessary concentrations. Thus, it is important to point out, that techniques focused on the electrode and those on the electrolyte complement each other very well. Additional investigations regarding the evolution of gases during aging and the role of the passive parts (the separator, current collector, binder, and conductive agents) would facilitate a complete study of decomposition processes within EDLCs. Further, individual aging processes could be assigned to one or a combination of several key components of EDLCs.

4. Conclusion

In this study, we presented for the first time the design and the use of an electrochemical three-electrode cell for *in-operando* gas chromatography-mass spectrometry analysis of the liquid electrolyte of electrochemical energy storage devices. We showed that by utilizing this cell it is possible to obtain a detailed time-resolved insight into the formation and possible causes of degradation products. Furthermore, the possibility to use the cell in a three-electrode configuration enables differentiation of processes occurring at the respective positive or negative electrodes.

The cell was utilized to investigate the behavior of EDLCs containing the conventional electrolyte 1 M $TEABF_4$ in ACN. Taking advantage of the unique features of the cell, it was possible to gain information about the degradation processes of ACN. Particularly, we showed that the degradation of this solvent is strongly affected by the surface chemistry of the respective electrode. However, a detailed investigation of varying different carbons (containing more acidic surface functions or less utilizing CDC materials) and different binders (PTFE, PvDF) is needed to determine the source of oxygen for the formation of acetamide derivates. Further, it has been determined, that the formation of acetamide derivates as well as the formation of the triazine derivate occurs at both, the positive and the negative electrodes. Furthermore, it was possible to identify the potential at which the electrodes begin to age, and we show that the aging of ACN-based EDLCs is mainly driven by the processes occurring at the positive electrode because this latter electrode is the first one that reaches an unstable potential.

Considering these results, the novel *in-operando* GC-MS cell reported in this work can be considered an innovative and very powerful tool for the investigation of the degradation processes taking place in electrochemical capacitors. Its use in combination with other *in-operando* techniques focused on the investigation of the gas phase (OEMS/DEMS), and the electrode (e.g. Raman or XPS) will allow a comprehensive *in-operando* investigation of aging processes occurring within EDLCs which, so far, was not possible. It is also important to remark that the cell

can be used for investigation of the interactions between different electrode materials in combination with a variety of electrolytes. For this reason, its use can be easily extended to the investigation of the aging processes occurring in batteries and fuel cells as well as for the investigation of electrocatalytic processes.

Credit author statement

Fabian Alexander Kreth and Lars Henning Heß, carried out the experimental work reported in the manuscript and wrote the article draft.

Andrea Balducci wrote/finalized the article and supervised the work of Fabian Alexander Kreth and Lars Henning Heß.

Declaration of Competing Interest

I declare that there are not conflict of interest related to the present manuscript.

I furthermore declare that this work has not been submitted previously to Energy Storage Materials (in part or in whole), that it has not been published previously an it is not under consideration for publication elsewhere, and is approved by all authors and host authorities.

Acknowledgment

The financial support from the Friedrich-Schiller-University Jena (FSU Jena) and Deutsche Forschungsgemeinschaft (DFG) within the project “New Electrolytes for Capacitive Electrochemical Storage” (BA4956/16-1) is gratefully acknowledged. We would like to thank Lukas Köps for fruitful discussions and IT support. Further, we would like to thank Marcus Ostermann, Christoph Weise, and co-workers for their help in the design and construction of the here-presented *in-operando* GC-MS cell.

Supplementary materials

Supplementary material associated with this article can be found, in the online version, at doi:10.1016/j.ensm.2023.01.014.

References

[1] J.B. Goodenough, K.S. Park, The Li-ion rechargeable battery: A perspective, J. Am. Chem. Soc. 135 (2013) 1167–1176, https://doi.org/10.1021/JA3091438/ASSET/IMAGES/MEDIUM/JA-2012-091438_0009.GIF.

[2] P. Simon, Y. Gogotsi, Perspectives for electrochemical capacitors and related devices, Nat. Mater. 19 (2020) 1151–1163, https://doi.org/10.1038/s41563-020-0747-z, 2020 1911.

[3] P. Kurzweil, M. Chwistek, Electrochemical stability of organic electrolytes in supercapacitors: Spectroscopy and gas analysis of decomposition products, J. Power Sources. 176 (2008) 555–567, https://doi.org/10.1016/j.jpowsour.2007.08.070.

[4] P.W. Ruch, D. Cericola, A. Foelske-Schmitz, R. Kötz, A. Wokaun, Aging of electrochemical double layer capacitors with acetonitrile-based electrolyte at elevated voltages, Electrochim. Acta. 55 (2010) 4412–4420, https://doi.org/10.1016/j.electacta.2010.02.064.

[5] P.W. Ruch, D. Cericola, A. Foelske, R. Kötz, A. Wokaun, A comparison of the aging of electrochemical double layer capacitors with acetonitrile and propylene carbonate-based electrolytes at elevated voltages, Electrochim. Acta. 55 (2010) 2352–2357, https://doi.org/10.1016/j.electacta.2009.11.098.

[6] M.M. Kabir, D.E. Demirocak, Degradation mechanisms in Li-ion batteries: a state-of-the-art review, Int. J. Energy Res. 41 (2017) 1963–1986, https://doi.org/10.1002/ER.3762.

[7] B. Pal, A. Yasin, R. Kaur, M. Tebyetekerwa, F. Zabihi, S. Yang, C.C. Yang, Z. Sofer, R. Jose, Understanding electrochemical capacitors with in-situ techniques, Renew. Sustain. Energy Rev. 149 (2021), 111418, https://doi.org/10.1016/J.RSER.2021.111418.

[8] A. Patra, K. N, J.R. Jose, S. Sahoo, B. Chakraborty, C.S. Rout, Understanding the charge storage mechanism of supercapacitors: in situ /operando spectroscopic approaches and theoretical investigations, J. Mater. Chem. A. 9 (2021) 25852–25891, https://doi.org/10.1039/D1TA07401F.

[9] Z. Lin, P.L. Taberna, P. Simon, Advanced analytical techniques to characterize materials for electrochemical capacitors, Curr. Opin. Electrochem. 9 (2018) 18–25, https://doi.org/10.1016/J.COELEC.2018.03.004.

[10] J.Z. Hu, N.R. Jaegers, M.Y. Hu, K.T. Mueller, In situ and ex situ NMR for battery research, J. Phys. Condens. Matter. 30 (2018), 463001, https://doi.org/10.1088/1361-648X/AAE5B8.

[11] A.M. Tripathi, W.N. Su, B.J. Hwang, In situ analytical techniques for battery interface analysis, Chem. Soc. Rev. 47 (2018) 736–751, https://doi.org/10.1039/C7CS00180K.

[12] H. Li, S. Guo, H. Zhou, In-situ/operando characterization techniques in lithium-ion batteries and beyond, J. Energy Chem. 59 (2021) 191–211, https://doi.org/10.1016/J.JECHEM.2020.11.020.

[13] P. Novák, J.C. Panitz, F. Joho, M. Lanz, R. Imhof, M. Coluccia, Advanced in situ methods for the characterization of practical electrodes in lithium-ion batteries, J. Power Sources. 90 (2000) 52–58, https://doi.org/10.1016/S0378-7753(00)00447-X.

[14] M.A. Bañares, Operando methodology: combination of in situ spectroscopy and simultaneous activity measurements under catalytic reaction conditions, Catal. Today. 100 (2005) 71–77, https://doi.org/10.1016/J.CATTOD.2004.12.017.

[15] Oxford English Dictionary, (n.d.). https://www.oed.com/ (accessed January 9, 2023).

[16] O. Munteshari, A. Borenstein, R.H. DeBlock, J. Lau, G. Whang, Y. Zhou, A. Likitchatchawankun, R.B. Kaner, B. Dunn, L. Pilon, In Operando Calorimetric Measurements for Activated Carbon Electrodes in Ionic Liquid Electrolytes under Large Potential Windows, ChemSusChem 13 (2020) 1013–1026, https://doi.org/10.1002/CSSC.201903011.

[17] O. Munteshari, J. Lau, A. Likitchatchawankun, B.A. Mei, C.S. Choi, D. Butts, B. S. Dunn, L. Pilon, Thermal signature of ion intercalation and surface redox reactions mechanisms in model pseudocapacitive electrodes, Electrochim. Acta. 307 (2019) 512–524, https://doi.org/10.1016/J.ELECTACTA.2019.03.185.

[18] O. Munteshari, J. Lau, D.S. Ashby, B. Dunn, L. Pilon, Effects of Constituent Materials on Heat Generation in Individual EDLC Electrodes, J. Electrochem. Soc. 165 (2018) A1547–A1557, https://doi.org/10.1149/2.0771807JES/XML.

[19] O. Munteshari, J. Lau, A. Krishnan, B. Dunn, L. Pilon, Isothermal calorimeter for measurements of time-dependent heat generation rate in individual supercapacitor electrodes, J. Power Sources. 374 (2018) 257–268, https://doi.org/10.1016/J.JPOWSOUR.2017.11.012.

[20] L.H. Hess, A. Bothe, A. Balducci, Design and Use of a Novel In Situ Simultaneous Thermal Analysis Cell for an Accurate “Real Time” Monitoring of the Heat and Weight Changes Occurring in Electrochemical Capacitors, Energy Technol 9 (2021), 2100329, https://doi.org/10.1002/ente.202100329.

[21] M. Hahn, R. Kötz, R. Gallay, A. Siggel, Pressure evolution in propylene carbonate based electrochemical double layer capacitors, Electrochim. Acta. 52 (2006) 1709–1712, https://doi.org/10.1016/j.electacta.2006.01.080.

[22] R. Kötz, M. Hahn, P. Ruch, R. Gallay, Comparison of pressure evolution in supercapacitor devices using different aprotic solvents, Electrochem. Commun. 10 (2008) 359–362, https://doi.org/10.1016/j.elecom.2007.12.016.

[23] M. He, K. Fic, E. Frackowiak, P. Novák, E.J. Berg, Ageing phenomena in high-voltage aqueous supercapacitors investigated by in situ gas analysis, Energy Environ. Sci. 9 (2016) 623–633, https://doi.org/10.1039/C5EE02875B.

[24] M. Hahn, A. Würsig, R. Gallay, P. Novák, R. Kötz, Gas evolution in activated carbon/propylene carbonate based double-layer capacitors, Electrochem. Commun. 7 (2005) 925–930, https://doi.org/10.1016/J.ELECOM.2005.06.015.

[25] N. Batisse, E. Raymundo-Piñero, Pulsed Electrochemical Mass Spectrometry for Operando Tracking of Interfacial Processes in Small-Time-Constant Electrochemical Devices such as Supercapacitors, ACS Appl. Mater. Interfaces. 9 (2017) 41224–41232, https://doi.org/10.1021/ACSAMI.7B12068/SUPPL_FILE/AM7B12068_SI_001.PDF.

[26] J. Ye, Y.C. Wu, K. Xu, K. Ni, N. Shu, P.L. Taberna, Y. Zhu, P. Simon, Charge Storage Mechanisms of Single-Layer Graphene in Ionic Liquid, J. Am. Chem. Soc. 141 (2019) 16559–16563, https://doi.org/10.1021/jacs.9b07134.

[27] W.Y. Tsai, P.L. Taberna, P. Simon, Electrochemical quartz crystal microbalance (EQCM) study of ion dynamics in nanoporous carbons, J. Am. Chem. Soc. 136 (2014) 8722–8728, https://doi.org/10.1021/ja503449w.

[28] N. Shpigel, M.D. Levi, S. Sigalov, L. Daikhin, D. Aurbach, In Situ Real-Time Mechanical and Morphological Characterization of Electrodes for Electrochemical Energy Storage and Conversion by Electrochemical Quartz Crystal Microbalance with Dissipation Monitoring, Acc. Chem. Res. 51 (2018) 69–79, https://doi.org/10.1021/ACS.ACCOUNTS.7B00477/ASSET/IMAGES/ACS.ACCOUNTS.7B00477.SOCIAL.JPEG_V03.

[29] M.D. Levi, L. Daikhin, D. Aurbach, V. Presser, Quartz Crystal Microbalance with Dissipation Monitoring (EQCM-D) for in-situ studies of electrodes for supercapacitors and batteries: A mini-review, Electrochem. Commun. 67 (2016) 16–21, https://doi.org/10.1016/J.ELECOM.2016.03.006.

[30] F. Escobar-Teran, A. Arnau, J.V. Garcia, Y. Jiménez, H. Perrot, O. Sel, Gravimetric and dynamic deconvolution of global EQCM response of carbon nanotube based electrodes by Ac-electrogravimetry, Electrochem. Commun. 70 (2016) 73–77, https://doi.org/10.1016/J.ELECOM.2016.07.005.

[31] C.R. Arias, C. Debiemme-Chouvy, C. Gabrielli, C. Laberty-Robert, A. Pailleret, H. Perrot, O. Sel, New insights into pseudocapacitive charge-storage mechanisms in Li-birnessite type MnO2 monitored by fast quartz crystal microbalance methods, J. Phys. Chem. C. 118 (2014) 26551–26559, https://doi.org/10.1021/JP508543H/SUPPL_FILE/JP508543H_SI_001.PDF.

[32] V. Dargel, N. Shpigel, S. Sigalov, P. Nayak, M.D. Levi, L. Daikhin, D. Aurbach, In situ real-time gravimetric and viscoelastic probing of surface films formation on lithium batteries electrodes, Nat. Commun. 8 (2017), https://doi.org/10.1038/S41467-017-01722-X.

[33] T. Liu, L. Lin, X. Bi, L. Tian, K. Yang, J. Liu, M. Li, Z. Chen, J. Lu, K. Amine, K. Xu, F. Pan, In situ quantification of interphasial chemistry in Li-ion battery, Nat.

Nanotechnol. 141 (14) (2018) 50–56, https://doi.org/10.1038/s41565-018-0284-y, 2018.
[34] S. Osswald, Y. Gogotsi, In situ Raman spectroscopy of oxidation of carbon nanomaterials. Raman Spectrosc. Nanomater. Charact., Springer, Berlin, Heidelberg, 2012, pp. 291–351, https://doi.org/10.1007/978-3-642-20620-7_12.
[35] C. Prehal, H. Fitzek, G. Kothleitner, V. Presser, B. Gollas, S.A. Freunberger, Q. Abbas, Persistent and reversible solid iodine electrodeposition in nanoporous carbons, Nat. Commun. 111 (11) (2020) 1–10, https://doi.org/10.1038/s41467-020-18610-6, 2020.
[36] C.M. Julien, A. Mauger, In situ Raman analyses of electrode materials for Li-ion batter, AIMS Mater. Sci. 5 (2018) 650–698, https://doi.org/10.3934/MATERSCI.2018.4.650.
[37] P. Lanz, P. Novák, Combined In Situ Raman and IR Microscopy at the Interface of a Single Graphite Particle with Ethylene Carbonate/Dimethyl Carbonate, J. Electrochem. Soc. 161 (2014) A1555–A1563, https://doi.org/10.1149/2.0021410JES/XML.
[38] R. Venâncio, R. Vicentini, L.H. Costa, R. Teófilo, L.M. Da Silva, H. Zanin, In-situ electrochemical and operando Raman techniques to investigate the effect of porosity in different carbon electrodes in organic electrolyte supercapacitors, J. Energy Storage. 50 (2022), 104219, https://doi.org/10.1016/J.EST.2022.104219.
[39] F.W. Richey, Y.A. Elabd, In situ molecular level measurements of ion dynamics in an electrochemical capacitor, J. Phys. Chem. Lett. 3 (2012) 3297–3301, https://doi.org/10.1021/JZ301422R/SUPPL_FILE/JZ301422R_SI_002.PDF.
[40] F.W. Richey, B. Dyatkin, Y. Gogotsi, Y.A. Elabd, Ion dynamics in porous carbon electrodes in supercapacitors using in situ infrared spectroelectrochemistry, J. Am. Chem. Soc. 135 (2013) 12818–12826, https://doi.org/10.1021/JA406120E/SUPPL_FILE/JA406120E_SI_001.PDF.
[41] F.W. Richey, C. Tran, V. Kalra, Y.A. Elabd, Ionic liquid dynamics in nanoporous carbon nanofibers in supercapacitors measured with in operando infrared spectroelectrochemistry, J. Phys. Chem. C. 118 (2014) 21846–21855, https://doi.org/10.1021/JP506903M/SUPPL_FILE/JP506903M_SI_001.PDF.
[42] J. Yang, N. Solomatin, A. Kraytsberg, Y. Ein-Eli, J. Yang, N. Solomatin, A. Kraytsberg, Y. Ein-Eli, In-Situ Spectro–electrochemical Insight Revealing Distinctive Silicon Anode Solid Electrolyte Interphase Formation in a Lithium–ion Battery, ChemistrySelect 1 (2016) 572–576, https://doi.org/10.1002/SLCT.201600119.
[43] Y. Akita, M. Segawa, H. Munakata, K. Kanamura, In-situ Fourier transform infrared spectroscopic analysis on dynamic behavior of electrolyte solution on LiFePO4 cathode, J. Power Sources. 239 (2013) 175–180, https://doi.org/10.1016/J.JPOWSOUR.2013.03.134.
[44] K. Hongyou, T. Hattori, Y. Nagai, T. Tanaka, H. Nii, K. Shoda, Dynamic in situ fourier transform infrared measurements of chemical bonds of electrolyte solvents during the initial charging process in a Li ion battery, J. Power Sources. 243 (2013) 72–77, https://doi.org/10.1016/J.JPOWSOUR.2013.05.192.
[45] J.M. Griffin, A.C. Forse, W.Y. Tsai, P.L. Taberna, P. Simon, C.P. Grey, In situ NMR and electrochemical quartz crystal microbalance techniques reveal the structure of the electrical double layer in supercapacitors, Nat. Mater. 14 (2015) 812–819, https://doi.org/10.1038/nmat4318.
[46] A.C. Forse, J.M. Griffin, C. Merlet, J. Carretero-Gonzalez, A.R.O. Raji, N.M. Trease, C.P. Grey, Direct observation of ion dynamics in supercapacitor electrodes using in situ diffusion NMR spectroscopy, Nat. Energy. 2 (2017) 1–7, https://doi.org/10.1038/nenergy.2016.216.
[47] Z.X. Luo, Y.Z. Xing, S. Liu, Y.C. Ling, A. Kleinhammes, Y. Wu, Dehydration of Ions in Voltage-Gated Carbon Nanopores Observed by in Situ NMR, J. Phys. Chem. Lett. 6 (2015) 5022–5026, https://doi.org/10.1021/acs.jpclett.5b02208.
[48] M. Deschamps, E. Gilbert, P. Azais, E. Raymundo-Piñero, M.R. Ammar, P. Simon, D. Massiot, F. Béguin, Exploring electrolyte organization in supercapacitor electrodes with solid-state NMR, Nat. Mater. 124 (12) (2013) 351–358, https://doi.org/10.1038/nmat3567, 2013.
[49] H. Wang, A.C. Forse, J.M. Griffin, N.M. Trease, L. Trognko, P.L. Taberna, P. Simon, C.P. Grey, In situ NMR spectroscopy of supercapacitors: Insight into the charge storage mechanism, J. Am. Chem. Soc. 135 (2013) 18968–18980, https://doi.org/10.1021/JA410287S/SUPPL_FILE/JA410287S_SI_003.MPG.
[50] L.H. Hess, N. Fulik, J. Röhner, E. Zhang, S. Kaskel, E. Brunner, A. Balducci, The role of diffusion processes in the self-discharge of electrochemical capacitors, Energy Storage Mater 37 (2021) 501–508, https://doi.org/10.1016/J.ENSM.2021.02.007.
[51] R. Bhattacharyya, B. Key, H. Chen, A.S. Best, A.F. Hollenkamp, C.P. Grey, In situ NMR observation of the formation of metallic lithium microstructures in lithium batteries, Nat. Mater. 96 (9) (2010) 504–510, https://doi.org/10.1038/nmat2764, 2010.
[52] K.A. Hirasawa, T. Sato, H. Asahina, S. Yamaguchi, S. Mori, In Situ Electrochemical Atomic Force Microscope Study on Graphite Electrodes, J. Electrochem. Soc 144 (1997) L81, https://doi.org/10.1149/1.1837560.
[53] X. Tao, J. Du, Y. Sun, S. Zhou, Y. Xia, H. Huang, Y. Gan, W. Zhang, X. Li, Exploring the Energy Storage Mechanism of High Performance MnO2 Electrochemical Capacitor Electrodes: An In Situ Atomic Force Microscopy Study in Aqueous Electrolyte, Adv. Funct. Mater. 23 (2013) 4745–4751, https://doi.org/10.1002/ADFM.201300359.
[54] Y. Guan, M. Zhang, J. Qin, X. Guo, Z. Li, B. Zhang, J. Tang, Morphological Evolutions of Ti3C2T xNanosheets and Fe3O4/Ti3C2T xNanocomposites under Potential Cycling Investigated Using in Situ Electrochemical Atomic Force Microscopy, J. Phys. Chem. C. 125 (2021) 12811–12818, https://doi.org/10.1021/ACS.JPCC.1C03167/SUPPL_FILE/JP1C03167_SI_001.PDF.
[55] H.J. Butt, B. Cappella, M. Kappl, Force measurements with the atomic force microscope: Technique, interpretation and applications, Surf. Sci. Rep. 59 (2005) 1–152, https://doi.org/10.1016/J.SURFREP.2005.08.003.
[56] X. Cui, L. Zhang, J. Zhang, L. Gong, M. Gao, P. Zheng, L. Xiang, W. Wang, W. Hu, Q. Xu, W. Wei, H. Zeng, A novel metal-organic layered material with superior supercapacitive performance through ultrafast and reversible tetraethylammonium intercalation, Nano Energy 59 (2019) 102–109, https://doi.org/10.1016/J.NANOEN.2019.02.034.
[57] J.M. Black, G. Feng, P.F. Fulvio, P.C. Hillesheim, S. Dai, Y. Gogotsi, P.T. Cummings, S.V Kalinin, N. Balke, Strain-Based In Situ Study of Anion and Cation Insertion into Porous Carbon Electrodes with Different Pore Sizes, Adv. Energy Mater. 4 (2014), 1300683, https://doi.org/10.1002/AENM.201300683.
[58] X. Wang, T.S. Mathis, K. Li, Z. Lin, L. Vlcek, T. Torita, N.C. Osti, C. Hatter, P. Urbankowski, A. Sarycheva, M. Tyagi, E. Mamontov, P. Simon, Y. Gogotsi, Influences from solvents on charge storage in titanium carbide MXenes, Nat. Energy. 4 (2019) 241–248, https://doi.org/10.1038/s41560-019-0339-9.
[59] Z. Lin, P. Rozier, B. Duployer, P.L. Taberna, B. Anasori, Y. Gogotsi, P. Simon, Electrochemical and in-situ X-ray diffraction studies of Ti3C2Tx MXene in ionic liquid electrolyte, Electrochem. Commun. 72 (2016) 50–53, https://doi.org/10.1016/j.elecom.2016.08.023.
[60] M.M. Hantel, R. Nesper, A. Wokaun, R. Kötz, In-situ XRD and dilatometry investigation of the formation of pillared graphene via electrochemical activation of partially reduced graphite oxide, Electrochim. Acta. 134 (2014) 459–470, https://doi.org/10.1016/j.electacta.2014.04.063.
[61] O. Ghodbane, J.L. Pascal, B. Fraisse, F. Favier, Structural in situ study of the thermal behavior of manganese dioxide materials: Toward selected electrode materials for supercapacitors, ACS Appl. Mater. Interfaces. 2 (2010) 3493–3505, https://doi.org/10.1021/AM100669K/ASSET/IMAGES/AM100669K.SOCIAL.JPEG_V03.
[62] O. Ghodbane, F. Ataherian, N.L. Wu, F. Favier, In situ crystallographic investigations of charge storage mechanisms in MnO 2-based electrochemical capacitors, J. Power Sources. 206 (2012) 454–462, https://doi.org/10.1016/J.JPOWSOUR.2012.01.103.
[63] J. Cheng, G.P. Cao, Y.S. Yang, Characterization of sol-gel-derived NiOx xerogels as supercapacitors, J. Power Sources. 159 (2006) 734–741, https://doi.org/10.1016/J.JPOWSOUR.2005.07.095.
[64] D. Manova, S. Mändl, In situ XRD measurements to explore phase formation in the near surface region, J. Appl. Phys. 126 (2019), 200901, https://doi.org/10.1063/1.5126636.
[65] S. Zhao, C. Chen, X. Zhao, X. Chu, F. Du, G. Chen, Y. Gogotsi, Y. Gao, Y. Dall'Agnese, Flexible Nb4C3Tx Film with Large Interlayer Spacing for High-Performance Supercapacitors, Adv. Funct. Mater. 30 (2020), 2000815, https://doi.org/10.1002/ADFM.202000815.
[66] F. Lin, Y. Liu, X. Yu, L. Cheng, A. Singer, O.G. Shpyrko, H.L. Xin, N. Tamura, C. Tian, T.C. Weng, X.Q. Yang, Y.S. Meng, D. Nordlund, W. Yang, M.M. Doeff, Synchrotron X-ray Analytical Techniques for Studying Materials Electrochemistry in Rechargeable Batteries, Chem. Rev 117 (2017) 13123–13186, https://doi.org/10.1021/ACS.CHEMREV.7B00007/ASSET/IMAGES/CR-2017-000073_M008.GIF.
[67] S. Chattopadhyay, A.L. Lipson, H.J. Karmel, J.D. Emery, T.T. Fister, P.A. Fenter, M. C. Hersam, M.J. Bedzyk, In situ X-ray study of the solid electrolyte interphase (SEI) formation on graphene as a model Li-ion battery anode, Chem. Mater. 24 (2012) 3038–3043, https://doi.org/10.1021/CM301584R/SUPPL_FILE/CM301584R_SI_001.PDF.
[68] J. Kruusma, A. Tõnisoo, R. Pärna, E. Nõmmiste, I. Tallo, T. Romann, E. Lust, Influence of the negative potential of molybdenum carbide derived carbon electrode on the in situ synchrotron radiation activated X-ray photoelectron spectra of 1-ethyl-3-methylimidazolium tetrafluoroborate, Electrochim. Acta. 206 (2016) 419–426, https://doi.org/10.1016/J.ELECTACTA.2015.10.060.
[69] J. Kruusma, A. Tõnisoo, R. Pärna, E. Nõmmiste, I. Kuusik, M. Vahtrus, I. Tallo, T. Romann, E. Lust, The Electrochemical Behavior of 1-Ethyl-3-Methyl Imidazolium Tetracyanoborate Visualized by In Situ X-ray Photoelectron Spectroscopy at the Negatively and Positively Polarized Micro-Mesoporous Carbon Electrode, J. Electrochem. Soc. 164 (2017) A3393, https://doi.org/10.1149/2.1861713JES.
[70] M.T. Camci, B. Ulgut, C. Kocabas, S. Suzer, In Situ XPS Reveals Voltage Driven Asymmetric Ion Movement of an Ionic Liquid through the Pores of a Multilayer Graphene Electrode, J. Phys. Chem. C. 122 (2018) 11883–11889, https://doi.org/10.1021/ACS.JPCC.8B02759/ASSET/IMAGES/ACS.JPCC.8B02759.SOCIAL.JPEG_V03.
[71] S. Wenzel, T. Leichtweiss, D. Krüger, J. Sann, J. Janek, Interphase formation on lithium solid electrolytes—An in situ approach to study interfacial reactions by photoelectron spectroscopy, Solid State Ionics 278 (2015) 98–105, https://doi.org/10.1016/J.SSI.2015.06.001.
[72] L. Köps, F.A. Kreth, A. Bothe, A. Balducci, High voltage electrochemical capacitors operating at elevated temperature based on 1,1-dimethylpyrrolidinium tetrafluoroborate, Energy Storage Mater 44 (2021) 66–72, https://doi.org/10.1016/j.ensm.2021.10.006.
[73] F.A. Kreth, A. Balucci, L.H. Hess, M. Ostermann, Method and Apparatus for the characterization of electrochemical devices in their operational timeframe, application number 102022002412. 8, 2022.
[74] L. Köps, F.A. Kreth, D. Leistenschneider, K. Schutjajew, R. Gläßner, M. Oschatz, A. Balducci, L. Köps, F.A. Kreth, D. Leistenschneider, K. Schutjajew, R. Gläßner, M. Oschatz, A. Balducci, Improving the Stability of Supercapacitors at High Voltages and High Temperatures by the Implementation of Ethyl Isopropyl Sulfone as Electrolyte Solvent, Adv. Energy Mater. (2022), 2203821, https://doi.org/10.1002/AENM.202203821.

[75] K.S. Teoh, M. Melchiorre, A. Fabian, A. Kreth, L. Bothe, F. Köps, A. Ruffo, Balducci, γ-Valerolactone as Sustainable and Low-Toxic Solvent for Electrical Double Layer Capacitors, ChemSusChem (2022), e202201845, https://doi.org/10.1002/CSSC.202201845.
[76] L. Köps, P. Zaccagnini, C.F. Pirri, A. Balducci, Determination of reliable resistance values for electrical double-layer capacitors, J. Power Sources Adv. 16 (2022), 100098, https://doi.org/10.1016/J.POWERA.2022.100098.
[77] A. Allagui, M.E. Fouda, Inverse problem of reconstructing the capacitance of electric double-layer capacitors, Electrochim. Acta. 390 (2021), 138848, https://doi.org/10.1016/J.ELECTACTA.2021.138848.
[78] J.M. Klein, E. Panichi, B. Gurkan, Potential dependent capacitance of [EMIM] [TFSI], [N 1114] [TFSI] and [PYR 13] [TFSI] ionic liquids on glassy carbon, Phys. Chem. Chem. Phys. 21 (2019) 3712–3720, https://doi.org/10.1039/C8CP04631J.
[79] P. Azaïs, L. Duclaux, P. Florian, D. Massiot, M.A. Lillo-Rodenas, A. Linares-Solano, J.P. Peres, C. Jehoulet, F. Béguin, Causes of supercapacitors ageing in organic electrolyte, J. Power Sources. 171 (2007) 1046–1053, https://doi.org/10.1016/j.jpowsour.2007.07.001.
[80] Y. Liu, B. Soucaze-Guillous, P.-L. Taberna, P. Simon, Understanding of carbon-based supercapacitors ageing mechanisms by electrochemical and analytical methods, J. Power Sources. 366 (2017) 123–130, https://doi.org/10.1016/J.JPOWSOUR.2017.08.104.
[81] Y. Liu, B. Réty, C. Matei Ghimbeu, B. Soucaze-Guillous, P.L. Taberna, P. Simon, Understanding ageing mechanisms of porous carbons in non-aqueous electrolytes for supercapacitors applications, J. Power Sources. 434 (2019), 226734, https://doi.org/10.1016/j.jpowsour.2019.226734.
[82] D. Bresser, D. Buchholz, A. Moretti, A. Varzi, S. Passerini, Alternative binders for sustainable electrochemical energy storage – the transition to aqueous electrode processing and bio-derived polymers, Energy Environ. Sci. 11 (2018) 3096–3127, https://doi.org/10.1039/C8EE00640G.
[83] N. Böckenfeld, S.S. Jeong, M. Winter, S. Passerini, A. Balducci, Natural, cheap and environmentally friendly binder for supercapacitors, J. Power Sources. 221 (2013) 14–20, https://doi.org/10.1016/J.JPOWSOUR.2012.07.076.
[84] A. Herrera, R. Martínez-Alvarez, P. Ramiro, M. Chioua, R. Chioua, A practical and easy synthesis of 2,4,6-trisubstituted-s-triazines, Synthesis (Stuttg) (2004) 503–505, https://doi.org/10.1055/S-2004-815927.
[85] T.L. Cairns, A.W. Larchar, B.C. McKusick, The Trimerization of Nitriles at High Pressures, J. Am. Chem. Soc. 74 (1952) 5633–5636, https://doi.org/10.1021/JA01142A028/ASSET/JA01142A028.FP.PNG_V03.
[86] T. Le Sueur Cairns, A.W. Larchar, B.C. McKusick, United States Patent: 2503999, 2503999, 1950. https://patft1.uspto.gov/netacgi/nph-Parser?Sect1=PTO1&Sect2=HITOFF&d=PALL&p=1&u=%2Fnetahtml%2FPTO%2Fsrchnum.htm&r=1&f=G&l=50&s1=2503999.PN.&OS=PN/2503999&RS=PN/2503999 (accessed June 10, 2022).
[87] F. Goettmann, A. Fischer, M. Antonietti, A. Thomas, Mesoporous graphitic carbon nitride as a versatile, metal-free catalyst for the cyclisation of functional nitriles and alkynes, New J. Chem. 31 (2007) 1455–1460, https://doi.org/10.1039/B618555J.
[88] M.I. Amer, B.L. Booth, G.F.M. Noori, M.F.J.R.P. Proença, The chemistry of nitrilium salts. Part 3. The importance of triazinium salts in Houben–Hoesch reactions catalyzed by trifluoromethanesulphonic acid, J. Chem. Soc. Perkin Trans. 1. 0 (1983) 1075–1082, https://doi.org/10.1039/P19830001075.
[89] J.H. Forsberg, V.T. Spaziano, S.P. Klump, K.M. Sanders, Lanthanide(III) ion catalyzed reaction of ammonia and nitriles: Synthesis of 2,4,6-trisubstituted-s-triazines, J. Heterocycl. Chem. 25 (1988) 767–770, https://doi.org/10.1002/JHET.5570250312.
[90] E.A. Kauck, J.H. Simons, U.S. Patent (1952) 927, 2 616.
[91] G.G.I. Moore, J.C. Hansen, T.M. Barrett, J.E. Waddell, K.M. Jewell, T.A. Kestner, R. M. Payfer, Electrochemical fluorination of aminoalkyl ethers, J. Fluor. Chem. 32 (1986) 41–76, https://doi.org/10.1016/S0022-1139(00)80506-0.
[92] Organikum, 24th ed., Wiley-VCH Verlag, Weinheim, 2015. https://www.wiley-vch.de/de/fachgebiete/naturwissenschaften/organikum-978-3-527-33968-6.
[93] M. Zhu, C.J. Weber, Y. Yang, M. Konuma, U. Starke, K. Kern, A.M. Bittner, Chemical and electrochemical ageing of carbon materials used in supercapacitor electrodes, Carbon N. Y. 46 (2008) 1829–1840, https://doi.org/10.1016/j.carbon.2008.07.025.
[94] A.M. Bittner, M. Zhu, Y. Yang, H.F. Waibel, M. Konuma, U. Starke, C.J. Weber, Ageing of electrochemical double layer capacitors, J. Power Sources. 203 (2012) 262–273, https://doi.org/10.1016/j.jpowsour.2011.10.083.
[95] Y. Liu, B. Soucaze-Guillous, P.L. Taberna, P. Simon, Understanding of carbon-based supercapacitors ageing mechanisms by electrochemical and analytical methods, J. Power Sources. 366 (2017) 123–130, https://doi.org/10.1016/j.jpowsour.2017.08.104.